AIP | Applied Physics Letters

Transient photoresponse of nitrogen-doped ultrananocrystalline diamond electrodes in saline solution

Arman Ahnood, Alexandr N. Simonov, Jamie S. Laird, Matias I. Maturana, Kumaravelu Ganesan, Alastair Stacey, Michael R. Ibbotson, Leone Spiccia, and Steven Prawer

Citation: Applied Physics Letters **108**, 104103 (2016); doi: 10.1063/1.4942976
View online: http://dx.doi.org/10.1063/1.4942976
View Table of Contents: http://scitation.aip.org/content/aip/journal/apl/108/10?ver=pdfcov
Published by the AIP Publishing

Transient photoresponse of nitrogen-doped ultrananocrystalline diamond electrodes in saline solution

Arman Ahnood,[1,a)] Alexandr N. Simonov,[2] Jamie S. Laird,[3] Matias I. Maturana,[4,5] Kumaravelu Ganesan,[1] Alastair Stacey,[1] Michael R. Ibbotson,[4,6] Leone Spiccia,[2] and Steven Prawer[1]

[1]*School of Physics, University of Melbourne, Melbourne, Victoria 3010, Australia*
[2]*School of Chemistry and the ARC Centre of Excellence for Electromaterials Science, Monash University, Melbourne, Victoria 3800, Australia*
[3]*CSIRO, Minerals Resources Flagship, School of Physics, University of Melbourne, Melbourne, Victoria 3010, Australia*
[4]*National Vision Research Institute, Australian College of Optometry, Carlton, Victoria 3053, Australia*
[5]*NeuroEngineering Laboratory, Department of Electrical and Electronic Engineering, University of Melbourne, Parkville, Victoria 3010, Australia*
[6]*ARC Centre of Excellence for Integrative Brain Function, Department of Optometry and Vision Sciences, University of Melbourne, Parkville, Victoria 3010, Australia*

(Received 21 December 2015; accepted 17 February 2016; published online 10 March 2016)

Beyond conventional electrically-driven neuronal stimulation methods, there is a growing interest in optically-driven approaches. In recent years, nitrogen-doped ultrananocrystalline diamond (N-UNCD) has emerged as a strong material candidate for use in electrically-driven stimulation electrodes. This work investigates the electrochemical activity of N-UNCD in response to pulsed illumination, to assess its potential for use as an optically-driven stimulation electrode. Whilst N-UNCD in the as-grown state exhibits a weak photoresponse, the oxygen plasma treated film exhibits two orders of magnitude enhancement in its sub-bandgap open circuit photovoltage response. The enhancement is attributed to the formation of a dense network of oxygen-terminated diamond nanocrystals at the N-UNCD surface. Electrically connected to the N-UNCD bulk via sub-surface graphitic grain boundaries, these diamond nanocrystals introduce a semiconducting barrier between the sub-surface graphitic semimetal and the electrolyte solution, leading to a photovoltage under irradiation with wavelengths of $\lambda = 450$ nm and shorter. Within the safe optical exposure limit of 2 mW mm^{-2}, charge injection capacity of 0.01 mC cm^{-2} is achieved using a 15×15 μm electrode, meeting the requirements for extracellular and intercellular stimulation. The nanoscale nature of processes presented here along with the diamond's biocompatibility and biostability open an avenue for the use of oxygen treated N-UNCD as optically driven stimulating electrodes. © *2016 AIP Publishing LLC*. [http://dx.doi.org/10.1063/1.4942976]

Direct optical stimulation of neurons, mediated *via* semiconducting photoabsorbers, is an emerging field with a number of potential applications in biomedical devices.[1] Traditionally, electrical stimuli delivered through electrically-driven extracellular or intercellular electrodes have been used to stimulate neurons. This differs from the optically-driven methods where the generation of a photocarrier in semiconducting photoabsorbers produces an electrical impulse for the stimulation of cells. Here, the semiconducting material plays the role of both a photoabsorber and an electrode. This method should also be distinguished from indirect optical stimulation approaches based on photodiodes connected to metallic electrodes.[2] One of the challenges encountered when using semiconducting materials for direct optical stimulation is their toxicity and long-term instability in the tissue.[1] From this perspective, diamond-based materials have shown remarkable properties, making them well suited for biological and medical applications.[3,4]

Ordinarily, a wide bandgap of single crystal diamond (5.5 eV, corresponding to the 225 nm limit for light absorption) inhibits photoresponses at wavelengths that are within the optical therapeutic window with wavelengths ranging from 320 to 800 nm.[5] Below this range, the interaction of light with tissue results in phototoxic reactions. Therefore, it is important to introduce a suitable mechanism for a sub-bandgap photosensitivity to the diamond for our proposed application. Use of either a diamond/graphite mixed phase material[6] or surface transfer doping[7] are two possible methods for achieving the target sub-bandgap photoresponse.

Surface transfer doping achieved by hydrogen-termination of a diamond surface[8] results in the sub-bandgap photoresponse in the form of injection of solvated electron into the aqueous electrolyte solution,[7] due to the negative electron affinity of the hydrogen-terminated diamond.[10] Although the sub-bandgap photoresponse itself is desirable, solvated electron injection into the solution is detrimental from the cellular stimulation perspective, as it compromises the long-term stability of the electrode and also leads to tissue damage.[9] Diamond with positive electron affinity can be achieved through oxygen termination of the surface.[10] This process is known to hinder the injection of solvated electrons generated under illumination and also leads to higher electrochemical stability.[11]

In the absence of hydrogen-termination at the surface of the diamond, graphitic phases within the diamond

a)arman.ahnood@unimelb.edu.au

microstructure play an important role in the sub-bandgap photoresponse. Owing to their mixed phase nature, nanocrystalline diamond based thin films exhibit a number of unique properties. The presence of a diamond phase in close proximity to a graphitic phase results in room temperature electrical conductivity and photoresponse at sub-bandgap wavelengths.[6] Earlier works suggest[13] that oxygen termination of the diamond surface allows retaining positive electron affinity and thereby suppressing electron transfers through the electrode-solution interface. This is circumstantially corroborated by sluggish kinetics of electrocatalytic reactions at the oxygen-terminated diamond compared to the as-grown, hydrogen terminated diamond.[12]

In this work, we explore the potential for the use of oxygen-terminated, nitrogen-doped ultrananocrystalline diamond (N-UNCD) as an optically driven stimulation electrode. Although there have been a number of reports looking at the photoelectrochemical response of diamond[12,13] and related materials,[14,15] the role of surface termination has not been addressed in sufficient detail. Furthermore, most of these works have focused on the steady-state photoresponse and have not fully explored the effect of mixed phase materials such as N-UNCD. Here, we investigated the transient photoresponse of the N-UNCD on time scales relevant to the cellular stimulation using pulsed laser illumination within a frequency range of 100 Hz to 40 kHz, which translates to the 10 ms to 25 μs pulse period. These fast photoelectrochemical measurements facilitated spatial mapping of the laser induced photovoltage, as well as investigation of photovoltage dependencies on the illumination intensity and frequency at a timescale relevant to the cellular stimulation. Additional insights into the nature of the processes governing the N-UNCD photoresponse are obtained using slow photoelectrochemical measurements using 30 s broadband and monochromic light pulses. The role of surface termination is examined and discussed. The N-UNCD material selected in this work has been used previously as an electrode material in electrically driven prostheses. It is a biocompatible nontoxic material with excellent long term stability in the body. In earlier studies, we have used this material as an electrode to deliver electrical stimuli to neurons[16] and demonstrated that it can be integrated with conventional complementary metal oxide silicon (CMOS) circuits.[17]

Fig. 1(a) illustrates a schematic of the measurement setup as well as a cross sectional view of the N-UNCD electrodes fabricated in this work. Details of the N-UNCD electrode fabrication have been reported previously.[18] Using a laser micromachining system, the N-UNCD film was pixelated into electrically isolated electrodes with dimensions of $120 \times 120\,\mu$m ($30\,\mu$m spacing $-150\,\mu$m pitch) and into a $15 \times 15\,\mu$m single electrode. Following this, the sample was treated with 25%/75% oxygen/argon plasma at 50 W power and a pressure of 0.4 mbar for 36 h. Given the high etch rate of the graphitic phase relative to the diamond phase, the oxygen plasma treatment resulted in the removal of graphite on the surface of the N-UNCD which is exposed to the plasma, as well as oxygen termination of the exposed diamond grains.[19] The extended plasma treatment may also have resulted in minimal etching of diamond grains at the N-UNCD surface. Nevertheless, the highly preferential etching ensures a N-UNCD surface with a self-terminating layer rich in oxygen-terminated nanodiamond grains, connected *via* subsurface graphitic grain boundaries to the bulk N-UNCD film. Fast photoelectrochemical measurements, including surface mapping, were performed in a custom-made setup housed in a dark and electrically shielded probe station on a floating air table. A 405 nm wavelength 50 mW laser (*Coherent*) was used as a light source; however, the intensity of light at the electrode surface was within the $50\,\mu$W–1mW range as measured using an optical power meter (Newport, Inc.). The laser beam was collimated onto the sample through a computer-controlled mirror and beam-splitter and was focused down using a lens to a spot of approximately $20\,\mu$m in diameter. The computer-controlled mirror adjusted the angle of the beam to allow a scan area of 0.5×0.5 mm. The laser beam intensity was modulated using a sinusoid signal provided by a SR830 lock-in-amplifier (*Stanford research systems*). The electrical response to the illumination was measured as a transient open-circuit voltage between N-UNCD electrodes relative to a platinum electrode, both immersed in a 0.15 M phosphate buffer (pH = 7.3) with added 0.13 M NaCl at ambient temperature. A high sensitivity lock in-amplifier (*LIA-MV-150, femto*) was used to detect the open circuit voltage amplitude and phase, herein referred to as open circuit photovoltage (OCPV), relative to the laser modulator signal as the lock-in reference. A data acquisition system (*National Instruments*) was used to map the open circuit voltage response for each laser scan location.

Slow photoelectrochemical measurements were undertaken in a conventional three-electrode photoelectrochemical cell connected to a Bio-Logic VSP Modular potentiostat. A 150 W xenon arc lamp equipped with an Oriel solar simulator and an AM 1.5 G filter was used as a light source. Neutral density filters were used to adjust the light intensity, while band pass filters with an average band-width of 10 nm were employed for measurements at defined wavelengths. Ag|AgCl|KCl(sat.) and Ti wire (separated from the working compartment by a glass frit) were immersed in the working electrolyte solution (aqueous 0.1 M NaCl) and used as reference and auxiliary electrodes, respectively.

Fig. 1(b) shows the SEM image of the pixelated N-UNCD electrode array. Five of these electrodes, indicated with the red boundary line, were short-circuited from the backside to each other and connected for measurement. Fig. 1(c) shows the spatial map of OCPV across an area covering these electrodes. The OCPV represents the shift in open-circuit potential (OCP) of the N-UNCD electrode in response to a pulsed illumination, measured with respect to a platinum quasi-reference electrode. The measurement was performed using an optical modulation frequency of 20 kHz and at an intensity of $620\,\mu$W at the electrolyte surface, corresponding to 1.97 W mm^{-2}. A negative 68° phase shift observed here suggests a capacitive process. The unconnected electrodes surrounding the cluster of the electrodes do not exhibit any response, and neither does the exposed insulating polycrystalline diamond (PCD) between the active electrodes.

Fig. 2(a) illustrates the dependence of the OCPV value, obtained using the smaller $15 \times 15\,\mu$m single electrode, on the illumination intensity and laser modulation frequency. Typically, the open circuit voltage of an electrochemical cell

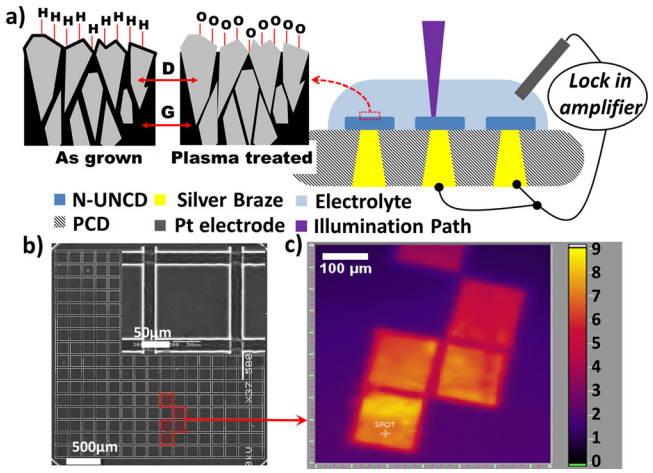

FIG. 1. (a) Cross sectional image of the N-UNCD electrode array fabricated on a polycrystalline diamond (PCD) and their connection to the lock-in-amplifier for OCPV measurements under pulsed 405 nm laser light. (b) SEM image of the N-UNCD electrode array; red dotted lines highlight 5 electrodes connected for the OCPV measurements. Inset shows a single $120 \times 120\,\mu$m electrode. (c) OCPV map of the N-UNCD electrodes array. The unconnected electrodes surrounding the cluster of the electrodes do not exhibit any response, and neither does the exposed PCD between the active electrodes.

follows a logarithmic dependence on the illumination intensity.[20] However, as shown in Fig. 2(a), there is a linear increase in the OCP amplitude with the increase in the illumination intensity for the N-UNCD electrode (power law dependence of 0.98 ± 0.13). Similar behaviour has been reported for other types of the state-of-the-art high-efficiency electrochemical cells at low illumination intensities (below 0.4 mW mm^{-2}).[21] The linear dependence of the OCPV on light intensity suggests that the device characteristics are dominated by recombination at localised mid-gap defect states.[20] As highlighted in Fig. 2(a), there is a reduction in the OCPV with an increase in frequency in the measurement range of 100 Hz to 40 kHz for all illumination intensities examined, which reflects the kinetics of the relevant photo-induced processes.

Fig. 2(b) illustrates the charge injection density per illumination pulse as a function of illumination intensity and modulation frequency assessed by adopting a method used in earlier works.[22] Here, the photo-induced current density as a function of frequency and illumination intensity is calculated

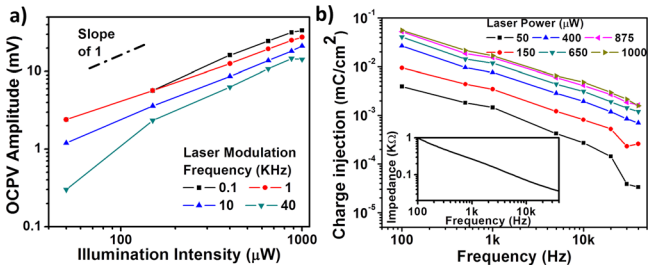

FIG. 2. OCPV for a single $15 \times 15\,\mu$m N-UNCD electrode as a function of (a) illumination intensity and modulation frequency using a 405 nm laser with a spot size of 20 μm diameter as a light source. Data are obtained using the fast photoelectrochemical measurement setup described in the text. (b) Calculated charge injection density per pulse of the N-UNCD electrode in response to the laser illumination under the open circuit conditions. Inset shows the magnitude of the electrochemical impedance measured at the open circuit voltage (potential amplitude 0.01 V) as a function of frequency.

as a ratio of the corresponding OCPV amplitude (Fig. 2(a)) and electrochemical impedance measured at the open-circuit potential (inset in Fig. 2(b)). Further, assuming a square wave of the irradiation pulse, the current density is divided by the illumination frequency to obtain the charge injection density per illumination pulse presented in Fig. 2(b).

To obtain further insights into the nature of the processes contributing to the detected OCPV, slow photoelectrochemical measurements were undertaken on the N-UNCD before and after plasma treatment. Under these conditions and using a 10 s light pulse with standard solar illumination spectrum at 1 mW mm^{-2} intensity, -13 mV OCPV was detected for the plasma treated N-UNCD, which is two orders of magnitude higher when compared to the OCPV for the as-grown N-UNCD (Fig. 3(a)). Another difference to note in the behaviour of the plasma treated and as-grown electrode is the opposite polarity of the OCPVs, *viz*. negative and positive, respectively (Fig. 3(a)).

Fig. 3(b) illustrates that the spectral response of the OCPV for the plasma treated N-UNCD sample exhibits a sharp reduction at wavelengths beyond 450 nm. Sub-bandgap photoassisted electron emission into vacuum from both single crystal diamond and UNCD has been reported.[23] At the macro-scale, the underlying mechanism for the sub-bandgap response has been attributed to the graphitic phases in these materials which provides a finite density of electrons at the Fermi level of the diamond.[23] At the same time, the diamond surface dominates the effective work function of the material[23] with hydrogen and oxygen terminations leading to a negative and positive electron affinity, respectively. The observed photoresponse at wavelengths of $\geq$450 nm ($h\nu > 2.76$ eV) is consistent with the $\pi \rightarrow \pi^*$ transition with an energy level of 2.1–2.5 eV.[24]

A nano-scale account of the photoresponse reported in this work can be provided based on a model proposed by Karabutov *et al.*[25] for graphite/nano-diamond/vacuum interfaces. Based on this, the N-UCND in contact with the electrolyte solution (Fig. 4(a)) can be considered as the intersection of three phases: (i) diamond nanocrystals, (ii) thin graphitic grain boundaries, and (iii) solution (electrolyte). The surface of the oxygen treated N-UNCD is dominated by a graphite/diamond/solution interface, as illustrated in Fig. 4(b). The oxygen-terminated N-UNCD film results in a positive electron affinity of 1.7 eV.[26] E_N represents the substitutional nitrogen providing deep donor states centred at an energy level of *ca* 1.7 eV.[27] The graphitic layer can be considered as a semimetal with a Fermi level of approximately $E_b = 4$ eV with respect to the diamond's conduction band.[28] Illumination at $h\nu > 2.76$ eV provides the required energy for the electrons from the graphitic grain boundaries to excite into and occupy diamond's photoionised nitrogen centres with energy level of $E_b - E_N = 4 - 1.7 = 2.3$ eV. The diamond/graphite schottky barrier[29] presented in Fig. 4(b) generates a photovoltage which leads to accumulation/orientation of charged-species in the electrolyte at the diamond/solution interface, which is subsequently observed as OCPV readout. Alternatively, it is possible for the E_b to be shifted towards the conduction band[29] due to a combination of quantum confinement in the nano-scale diamond size[30] and surface induced field in the junction,[29] resulting in the

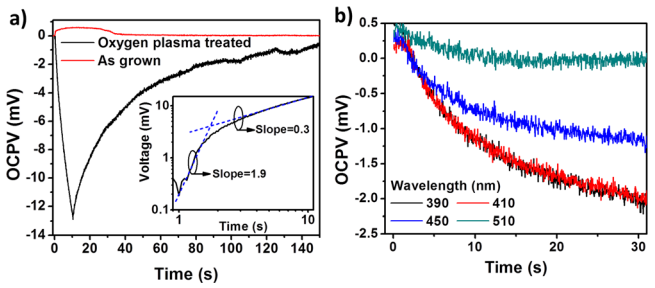

FIG. 3. (a) OCPV for the as-grown (red) and O_2/Ar plasma treated (black) N-UNCD electrode illuminated using a broadband 1×1.5AM sun (1 mW mm^{-2}) irradiation (from 0 to 10 s). Inset shows the OCPV magnitude for plasma treated N-UNCD in bi-logarithmic coordinates with two different kinetic regions approximated by the dashed lines. (b) OCPV for the plasma treated N-UNCD electrode under monochromatic irradiation indicating a diminishing response at wavelengths below 450 nm (2.76 eV). Data here are obtained using the slow photoelectrochemical measurement setup described in the text.

accumulation of electrons in the conduction band of the nanodiamond in response to $hv > 2.76$ eV.

As shown in Fig. 3(a), the OCPV is negative in the case of the oxygen/argon plasma treated N-UNCD, whereas it is positive for the N-UNCD in the as-grown state. Compared to the as-grown sample, oxygen plasma treatment results in two key changes: (a) the oxygen termination of the surface and (b) etching of the graphitic phases at the surface. Accumulation of the photoexcited electrons in the oxygen-terminated nanodiamond capping layer grains results in a more negatively charged surface and, hence, produces negative OCPV. However, in the case of as-grown, hydrogen terminated N-UNCD, the negative electron affinity of the surface results in the injection of the generated photoexcited electrons into the solution.[7] This inhibits the accumulation of the charge in the N-UNCD surface, manifested in a two orders of magnitude reduction in the OCPV, as well as the possibility of a slightly positive value due to the surface chemical reactions. This is consistent with both the direction (positive) and magnitude of the OCPV (0.5 mV) reported for as-grown boron doped polycrystalline diamond.[31]

The rate of the OCPV rise at the oxygen-terminated diamond electrodes is limited by two possible processes at different timescales: (1) initially, the rate of space-charge formation at the N-UNCD surface and, subsequently, (2) the rate of the surface-confined electrochemical processes. The formation of the space-charge regions in diamond at room temperature is typically on a timescale that is much shorter than the electrochemical processes. The OCPV measurement

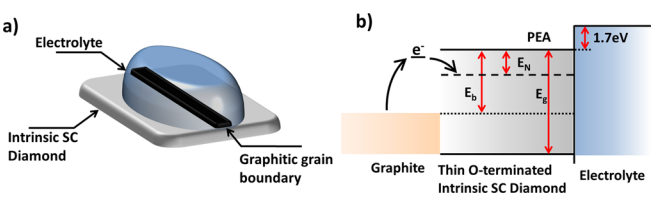

FIG. 4. (a) A schematic of the N-UNCD electrode in contact with the electrolyte solution, highlighting the presence of three different phases. (b) A putative band diagram of the graphite/diamond/solution interface for an oxygen terminated diamond surface. E_{NV} shows trap centres related to nitrogen donor states, E_b is the barrier between the graphite and diamond conduction bands (4 eV), PEA is positive electron affinity of 1.7 eV, E_g is the bandgap of the diamond (5.5 eV), and black arrows show putative electron pathway under irradiation.

at laser modulation frequencies of 100 Hz–40 kHz (as shown in Figs. 2(a) and 2(b)) is within the timescale required for the space-charge formation. This is also consistent with the observed negative 68° phase shift (i.e., capacitive) at these modulation frequencies.

The results shown in the inset to Fig. 3(a), obtained using the slow electrochemical measurements, are on a timescale that can only be attributed to the surface-confined electrochemical processes at the plasma treated N-UNCD electrode. Here, an initial sharp rise in the OCPV over the initial few seconds with a power law dependence of 1.9 is followed by a slower increase over the next *ca* 10 s with a power law dependence of 0.3. Oxygen-rich surface functionalities, such as carboxylic acid or hydroxyl, found on oxygen terminated diamond undergo an initial ionisation process when in contact with the electrolyte solution.[32] Once an equilibrium state is reached, further photo-induced reduction in these surface functionalities is possible. This can be driven either by the change in the diamond's surface potential relative to the electrolyte due to the space-charge formation or by further ionisation of the surface oxygen functionalities, where oxygen induced surface states[33] with a matching ~2.4 eV (Ref. 34) may have a role. Although the precise mechanism giving rise to the observed slow OCPV response is unclear, light induced change in the surface potential can slowly reduce the oxygen-rich functionalities on the plasma treated diamond surface. Upon ceasing the irradiation, the OCPV slowly relaxes to the close-to-initial state (over several minutes), reflecting the reversibility of the relevant photo-induced processes.

The charge density in Fig. 2(b) can be used to assess the viability of the plasma treated N-UNCD for cellular stimulation. By using the approach explained above, the photoinduced charge density for 100 Hz laser stimulation (i.e., 10 ms pulse period) is 0.004–0.051 mC cm^{-2} for the laser power of 50–1000 μW, respectively. The safe exposure limit of human tissue to light with wavelengths of 400–700 nm over extended periods of time is 2 mW mm^{-2}.[35] Based on this, a maximum average laser power of 1.25 μW can be used for the examined electrode geometry. Assuming a pulse duration of 1 ms per 500 ms (2 Hz pulse train[36,37] with a duty cycle of 0.5%), this corresponds to a power limit of 625 μW at 1 kHz. As shown in Fig. 2, this corresponds to a charge density of 0.01 mC cm^{-2}. The threshold for cellular stimulation, typically expressed as charge injection threshold, is strongly dependent on the type of cells being stimulated, placement of the stimulating electrode relative to the cell, and the stimulation parameters used. Table I provides an illustrative summary of the charge density required to perform stimulation in various cells. These data suggest that the 0.01 mC cm^{-2} charge density is within the threshold for some types of extracellular stimulation. Further enhancement in the photoresponse may be possible through reduction of the defect centres by process modification as well as optimising the frequency and duty cycle. Furthermore, the nanoscale nature of the effects observed here makes it possible to exploit this effect for intracellular stimulation.[38] The possibility of nanodiamond internalisation in living cells[39] might eventually lead to the placement of the optically controlled intracellular stimulation. Although the role of vesicles is unclear, charge

TABLE I. Comparison of the charge density at the N-UNCD within the safe exposure limit, and the relevant stimulation setting, with the threshold of required charge density for neuronal stimulation. Cases A and B are *in vivo* retinal stimulation performed in epiretinal and subretinal spaces, respectively. Case C is suggested parameters for *in vivo* brain stimulation. Case D is calculated based on *in vitro* neuronal tissue stimulation using intracellular electrode.

	This work	Case A[40]	Case B[41]	Case C[38]
Threshold (mC/cm^2)	0.01	0.023	0.0023–0.0067	0.001
Extra/intercellular	N/A	Extra-cellular	Extra-cellular	intracellular
Tissue/placement	N/A	Retina/subretinal	Deep brain stimulation	*In vitro* neuronal
Pulse duration (ms)	1	0.1–1	0.06–0.2	2.5
Size (μm)	15	40	1500	3

densities as low as 0.001 mC cm^{-2} are required[38] for intracellular stimulation.

In summary, this work reports transient photoresponses of N-UNCD in saline electrolyte solution within the tissues therapeutical optical window. The weak positive OCPV of the hydrogen-terminated, as-grown N-UNCD is attributed to its negative electron affinity, resulting in a thermodynamically favourable solvated electron injection into the electrolyte. Conversely, the oxygen plasma treated N-UNCD exhibits two orders of magnitude enhancement in its OCPV as well as a reversal of the voltage polarity. This enhancement is attributed to the formation of a dense network of oxygen-terminated diamond nanocrystals on the N-UNCD surface, which acts as a charge accumulation layer. The positive electron affinity of the oxygenated diamond surface makes the injection of solvated electrons into the solution less favourable.

Electrochemical processes strongly dominate the rate of the OCPV change in response to illumination pulses, resulting in a significant pulse duration dependence of the OCPV magnitude. As evident from the slow transient measurements, performance of the material is likely to be improved with further understanding of the trapping mechanisms and subsequent material fabrication optimisation processes, opening the door to more extracellular stimulation applications. Also, further investigation in the chemical stability and biocompatibility of photo-illuminated oxygen terminated diamond is needed to establish the lifetime of these electrodes in biological environments. Nevertheless, as demonstrated in this work, within the safe exposure limit using 1 ms illumination, the accumulated charge density is sufficient for some extracellular and intercellular stimulation regimes. Importantly, the nanoscale nature of processes present here along with the diamond's biocompatibility and biostability open an avenue for the use of oxygen treated N-UNCD, as well as other nano-scaled diamond electrodes for optically driven stimulation.

[1]L. Bareket-Keren and Y. Hanein, Int. J. Nanomedicine **9**(1), 65–83 (2014).
[2]H. Hämmerle, K. Kobuch, K. Kohler, W. Nisch, H. Sachs, and M. Stelzle, Biomaterials **23**(3), 797–804 (2002).
[3]L. Tang, C. Tsai, W. W. Gerberich, L. Kruckeberg, and D. R. Kania, Biomaterials **16**(6), 483–488 (1995).
[4]C. G. Specht, O. A. Williams, R. B. Jackman, and R. Schoepfer, Biomaterials **25**(18), 4073–4078 (2004).
[5]J. A. Parrish, J. Invest. Dermatol. **77**(1), 45–50 (1981).
[6]V. Seshan, D. H. K. Murthy, A. Castellanos-Gomez, S. Sachdeva, H. A. Ahmad, S. D. Janssens, W. Janssen, K. Haenen, H. S. J. van der Zant, E. J. R. Sudhölter, T. J. Savenije, and L. C. P. M. de Smet, ACS Appl. Mater. Interfaces **6**(14), 11368–11375 (2014).
[7]D. Zhu, L. Zhang, R. E. Ruther, and R. J. Hamers, Nat. Mater. **12**(9), 836–841 (2013).
[8]P. Strobel, M. Riedel, J. Ristein, and L. Ley, Nature **430**(6998), 439–441 (2004).
[9]D. R. Merrill, M. Bikson, and J. G. R. Jefferys, J. Neurosci. Methods **141**(2), 171–198 (2005).
[10]F. Maier, J. Ristein, and L. Ley, Phys. Rev. B **64**(16), 165411 (2001).
[11]G. R. Salazar-Banda, L. S. Andrade, P. A. P. Nascente, P. S. Pizani, R. C. Rocha-Filho, and L. A. Avaca, Electrochim. Acta **51**(22), 4612–4619 (2006).
[12]K. Patel, K. Hashimoto, and A. Fujishima, J. Photochem. Photobiol. Chem. **65**(3), 419–429 (1992).
[13]Y. V. Pelskov, A. Y. Sakharova, M. D. Krotova, L. L. Bouilov, and B. V. Spitsyn, J. Electroanal. Chem. Interfacial Electrochem. **228**(1–2), 19–27 (1987).
[14]A. Y. Sakharova, Y. V. Pleskov, F. D. Quarto, S. Piazza, C. Sunseri, I. G. Teremetskaya, and V. P. Varnin, J. Electrochem. Soc. **142**(8), 2704–2709 (1995).
[15]A. D. Modestov, J. Gun, and O. Lev, J. Electroanal. Chem. **476**(2), 118–131 (1999).
[16]D. J. Garrett, K. Ganesan, A. Stacey, K. Fox, H. Meffin, and S. Prawer, J. Neural Eng. **9**(1), 016002 (2012).
[17]A. Ahnood, M. C. Escudie, R. Cicione, C. D. Abeyrathne, K. Ganesan, K. E. Fox, D. J. Garrett, A. Stacey, N. V. Apollo, S. G. Lichter, C. D. L. Thomas, N. Tran, H. Meffin, and S. Prawer, Biomed. Microdevices **17**(3), 1–11 (2015).
[18]K. Ganesan, D. J. Garrett, A. Ahnood, M. N. Shivdasani, W. Tong, A. M. Turnley, K. Fox, H. Meffin, and S. Prawer, Biomaterials **35**(3), 908–915 (2014).
[19]H. Notsu, I. Yagi, T. Tatsuma, D. A. Tryk, and A. Fujishima, J. Electroanal. Chem. **492**(1), 31–37 (2000).
[20]P. Salvador, M. G. Hidalgo, A. Zaban, and J. Bisquert, J. Phys. Chem. B **109**(33), 15915–15926 (2005).
[21]T. M. W. J. Bandara, W. J. M. J. S. R. Jayasundara, H. D. N. S. Fernado, M. A. K. L. Dissanayake, L. A. A. D. Silva, I. Albinsson, M. Furlani, and B.-E. Mellander, J. Appl. Electrochem. **45**(4), 289–298 (2015).
[22]W. Wang, K. Foley, X. Shan, S. Wang, S. Eaton, V. J. Nagaraj, P. Wiktor, U. Patel, and N. Tao, Nat. Chem. **3**(3), 249–255 (2011).
[23]J. B. Cui, J. Ristein, and L. Ley, Phys. Rev. B **60**(23), 16135–16142 (1999).
[24]P. Achatz, J. A. Garrido, M. Stutzmann, O. A. Williams, D. M. Gruen, A. Kromka, and D. Steinmüller, Appl. Phys. Lett. **88**(10), 101908 (2006).
[25]A. V. Karabutov, V. D. Frolov, and V. I. Konov, Diamond Relat. Mater. **10**(3–7) 840–846 (2001).
[26]J. Ristein, Appl. Phys. A **82**(3), 377–384 (2005).
[27]H. B. Dyer, F. A. Raal, L. D. Preez, and J. H. N. Loubser, Philos. Mag. **11**(112), 763–774 (1965).
[28]T. Zimmermann, M. Kubovic, A. Denisenko, K. Janischowsky, O. A. Williams, D. M. Gruen, and E. Kohn, Diamond Relat. Mater. **14**(3–7), 416–420 (2005).
[29]J. Robertson and M. J. Rutter, Diamond Relat. Mater. **7**(2–5), 620–625 (1998).
[30]P.-H. Chung, E. Perevedentseva, and C.-L. Cheng, Surf. Sci. **601**(18), 3866–3870 (2007).
[31]Y. Pleskov, in *Diamond and Diamond-Like Film Applications* (CRC Press, 1998), pp. 90–96.
[32]V. Chakrapani, J. C. Angus, A. B. Anderson, S. D. Wolter, B. R. Stoner, and G. U. Sumanasekera, Science **318**(5855), 1424–1430 (2007).
[33]S. J. Sque, R. Jones, and P. R. Briddon, Phys. Rev. B **73**(8), 085313 (2006).
[34]Y. Itoh, Y. Sumikawa, H. Umezawa, and H. Kawarada, Appl. Phys. Lett. **89**(20), 203503 (2006).
[35]F. C. Delori, R. H. Webb, and D. H. Sliney, J. Opt. Soc. Am. A **24**(5), 1250–1265 (2007).
[36]R. G. McCaughey, C. Chlebicki, and B. J. F. Wong, Lasers Surg. Med. **42**(1), 69–75 (2010).
[37]A. D. Izzo, J. T. Walsh, E. D. Jansen, M. Bendett, J. Webb, H. Ralph, and C.-P. Richter, IEEE Trans. Biomed. Eng. **54**(6), 1108–1114 (2007).
[38]J. T. Robinson, M. Jorgolli, A. K. Shalek, M.-H. Yoon, R. S. Gertner, and H. Park, Nat. Nanotechnol. **7**(3), 180–184 (2012).
[39]C.-C. Fu, H.-Y. Lee, K. Chen, T.-S. Lim, H.-Y. Wu, P.-K. Lin, P.-K. Wei, P.-H. Tsao, H.-C. Chang, and W. Fann, Proc. Natl. Acad. Sci. **104**(3), 727–732 (2007).
[40]Y. Yamauchi, L. M. Franco, D. J. Jackson, J. F. Naber, R. O. Ziv, J. F. Rizzo III, H. J. Kaplan, and V. Enzmann, J. Neural Eng. **2**(1), S48 (2005).
[41]A. M. Kuncel and W. M. Grill, Clin. Neurophysiol. **115**(11), 2431–2441 (2004).